 doi:10.20944/preprints201804.0100.v1

Article

Modulatory effect of polyphenolic compounds from the mangrove tree *Rhizophora mangle* L. improving non-alcoholic fatty liver disease and insulin resistance in high-fat diet obese mice

Leonardo Mendes de Souza Mesquita [1], Cíntia Rabelo e Paiva Caria[2], Paola Souza Santos[2], Caio Cesar Ruy[2], Natalia da Silva Lima[2], Débora Kono Taketa Moreira[2], Claudia Quintino da Rocha[3]*, Daniella Carisa Murador[4], Veridiana Vera de Rosso[4], Alessandra Gambero[2] and Wagner Vilegas*

[1] Laboratory of Bioprospection of Natural Products (LBPN), UNESP - São Paulo State University/Coastal Campus of São Vicente, São Vicente, São Paulo, Brazil; mesquitalms@gmail.com (LMSM)
[2] Clinical Pharmacology and Gastroenterology Unit, USF – São Francisco University, Bragança Paulista, São Paulo, Brazil; alessandra.gambero@usf.edu.br
[3] Laboratory of Phytomedicine Advanced Studies (LEAF), UFMA- Federal University of Maranhão, São Luís, Maranhão, Brazil; claudiarocha3@yahoo.com.br
[4] Department of Biosciences, Federal University of São Paulo (UNIFESP), Santos, São Paulo, Brazil; veriderosso@yahoo.com

* Correspondence: claudiarocha3@yahoo.com.br; Tel.: +55-98-3272-9243

Abstract: *Rhizophora mangle* L. is a well-known medicinal plant found in mangroves worldwide used to treatment diabetes. This study evaluated the chemical composition of the acetonic extract from *Rhizophora mangle* barks (AERM), by HPLC-PDA and FIA-ESI-IT-MS/MS and the effects on high-fat diet induced obesity in mice and its mechanism of action by gene expression of inflammatory markers (*Pparg*, *Ppara*, *Srebf1*, *Cd36*, *Tnf*, *Ccl2*, *Lep*, *Il10*, *Il6*, *Fasn*, *18s*). High-fat diet fed mice during 12 weeks was used as model of obesity and associated alterations. The results were very satisfactory, the extract, rich in polyphenolic compounds, flavonoids and phenolic acids, displayed intense antioxidant activity *in vitro* (608 μmol Trolox/g), and showed excellent activity against non-alcoholic fatty liver disease (NAFLD) and reverse insulin resistance in a model of diet-induced obesity. We can registered a modulatory effect of AERM in liver PPAR-γ mRNA expression associated to an important inhibition of CD36 mRNA expression suggesting that AERM induces the down regulation of CD36 mRNA via PPAR-gamma inhibition. These results support the traditional knowledge about the use of *R. mangle* for the treatment of type 2 diabetes and reveal the potential of AERM for the treatment of NAFLD and management of obesity and comorbidities.

Keywords: Cd36; mass spectrometry; NAFLD; anti-lypase activity; anti-amylase activity; insulin resistance.

1. Introduction

Type 2 diabetes mellitus (T2D) is one of the major public health problems worldwide and the prevalence have been steadily increasing over the past few decades [1]. About 60% of Brazilian people are overweight or obese and associated diseases such as T2D and non-alcoholic fatty liver disease (NAFLD) are increasingly prevalent in Brazilian population [2]. The treatment and management of diabetes is usually performed by pharmacological drugs, which can cause side effects, such as weight gain, edema, hypoglycemia, lactic acidosis, liver toxicity, and gastrointestinal

 doi:10.20944/preprints201804.0100.v1

disturbances after long term use [3]. A recommended alternative for the diabetes treatment is the use of traditional medicinal plants [4].

Several medicinal plants are applied as complementary therapy for diabetic treatment, however, studies that reveal the efficacy and safety are still inscipient [5]. Many publications in Mexico and Latin America started to explore the use of medicinal plants by modern populations [6]. In this context, according to Andrade-Cetto & Heinrich, (2005) the barks of *Rhizophora mangle* L. (Rhizophoraceae) are widely reported as antidiabetic in traditional Mexican medicine. Besides that, *R. mangle* is commonly used in Latin America to treat inflammation, angina, asthma, pain, diarrhea, ulcers, tumors and seizures [8,9].

Rhizophora mangle L. (Rhizophoraceae) is one of the most prominent species in Brazilian mangrove ecosystems, which represent an unexplored source of secondary metabolites, which have a huge medicinal potential [10]. Phenolic compounds are the main source of phytochemicals found in mangrove plants, especially condensed tannins [11]; its barks are constituted by proanthocyanidins (PAs), oligomers and polymers by flavan-3-ol, which have intense antioxidant and anti-inflammatory activity [12]. PAs are widely distributed in the plant kingdom and are the second-most frequent phenolic substances, after lignins [13]. Polyphenols of plant origin are also capable of preventing both obesity and adipose tissue inflammation, improving obesity-associated metabolic syndrome in human subjects and animal models of obesity [14]. Our research group has already carried out excellent results with the use of *R. mangle* acetone extract (AERM) for the treatment and prevention of gastrointestinal diseases [11,15]. However, a more detailed chemical analysis from AERM is still necessary in order to characterize the main chemical constituents.

Considering these facts, in this study we characterized the chemical composition of the standardized AERM and we investigated the effect of AERM in improving glucose homeostasis, adipose tissue inflammation and hepatic steatosis in an experimental model diet-induced obesity in mice. In addition, the potential antioxidant, anti-amylase and anti-lipase of extract was also evaluated *in vitro*.

2. Results and discussion

2.1 Chemical characterization of the extract

In order to obtain the most useful chemical information and best separation in the fingerprint chromatograms of AERM, the mobile phase compositions, gradient elution procedure and detection wavelength were optimized. With the aim of enhancing the resolution, glacial formic acid (FA) was added to the binary mixture of methanol–water. To acquire better selectivity and higher efficiency, different concentrations of FA (0.05%, 0.1% and 0.5%) in the aqueous phase were also investigate. The mobile phase consisting of water-0.1% FA solution was chosen for the determination of AERM with large number of peaks on the chromatogram within 70 min. The wavelength was also optimized in order to obtain the highest number of the compounds detected.

Using the optimized HPLC-PDA method, we obtained baseline resolution. We could observe the presence of seven main peaks in AERM, with maximum absorbance values around 232 nm and 278 nm, which covered more than 90 % of the total area chromatogram (Figure 1A). Based on the UV spectrum of each chromatographic peaks (1-7) (Figure 1B), the constituents of AERM could be classified as catechin derivatives (λ_{max} 280 nm), which can polymerize, forming condensed tannins, known as proanthocyanidins (PA) [16]. Another fact that corroborates the presence of condensed tannins in this extract is the presence of a low chromatographic resolution peak eluting between R_t 55-70 min. The presence of tannins is common in plants occurring in the mangrove ecosystem [17]. In fact, Oo et al. (2008) [18] and Zhang et al. (2010) [19] described the occurrence of catechins, epicatechins and epigalocatechins in *R. apiculata* and *R. mangle*.

Preprints (www.preprints.org) | NOT PEER-REVIEWED | Posted: 9 April 2018 doi:10.20944/preprints201804.0100.v1

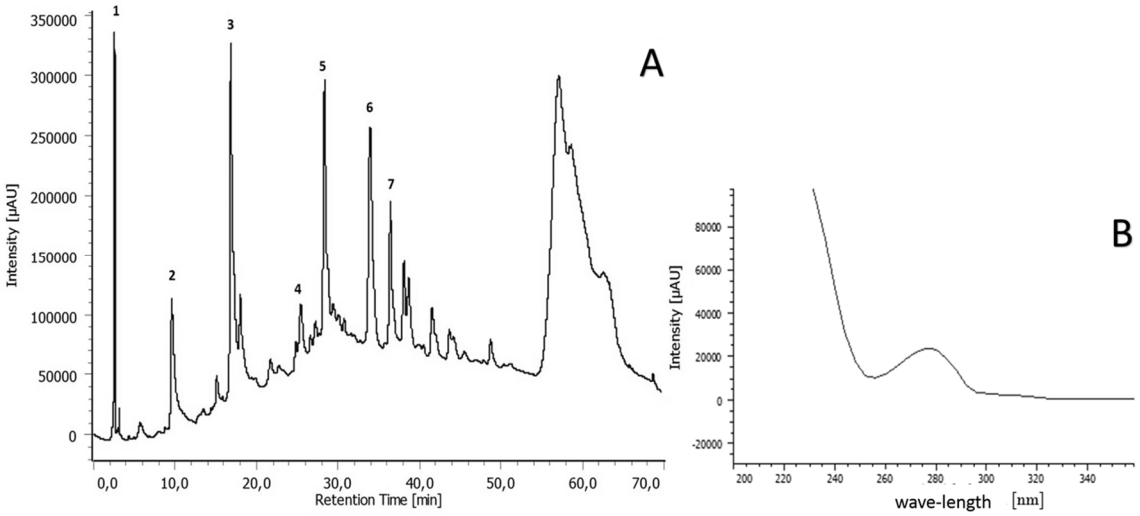

Figure 1. Compounds detected in the AERM (210 nm). Analytical HPLC-PAD chromatogram **(A)** and the corresponding UV spectra (peaks 1-7) **(B)**.

However, HPLC-PDA analyses were not enough to fully characterize the condensed tannins in AERM. According to Li et al. (2007) [20], ESI-MS techniques have been used efficiently for the characterization of several natural compounds, mainly polyphenolic compounds. Besides, MS/MS fragmentation of the flow injection analysis electrospray-iontrap mass spectrometry (FIA-ESI-IT-MS/MS) can generate product ions that give additional information about the structure of these compounds. FIA-ESI-IT-MS/MS were already applied to establish the polyphenol profile of complex matrices [21]. Thus, we decided to use this technique in order to obtain a qualitative metabolic fingerprint of the AERM, after a clean-up using SPE

In order to obtain qualitative information on PA in *R. mangle* extract, a sample rich of these compounds was prepared and directly injected into ESI source of the mass spectrometer. We tested both positive and negative ionization. The best results were obtained using negative mode. It was already reported that negative ionization is more sensitive and selective than the positive one [22]. Figure 2 and Table 1 show the ESI-MS fingerprint obtained using full scan, indicating the $[M-H]^-$ ions of the compounds present in the extract. After MS/MS experiments with each peak observed in the full scan spectrum, three main fragmentation mechanisms were observed: Retro-Diels-Alder (RDA), Quinone Methide (QM) and Heterocyclic Ring Fission (HRF) [23]. The fragmentation patterns obtained evidenced the presence of three series of polymeric proanthocyanidins. In the full scan experiment, the *m/z* 289 ion represents a unit of catechin. Besides, we also observed a first series of ions separated by 288 Da corresponding to ion peaks of dimeric (*m/z* 577) and trimeric (*m/z* 865) PA. We detected a second series of PA, based on a catechin core linked to hexose moieties (*m/z* 451: monomer; *m/z* 739: dimer). A third series of PAs is represented by catechins linked to deoxyhexose moieties (*m/z* 435: monomer; *m/z* 723: dimer). In order to check the possibilities, MS/MS experiments were performed.

Preprints (www.preprints.org) | NOT PEER-REVIEWED | Posted: 9 April 2018 doi:10.20944/preprints201804.0100.v1

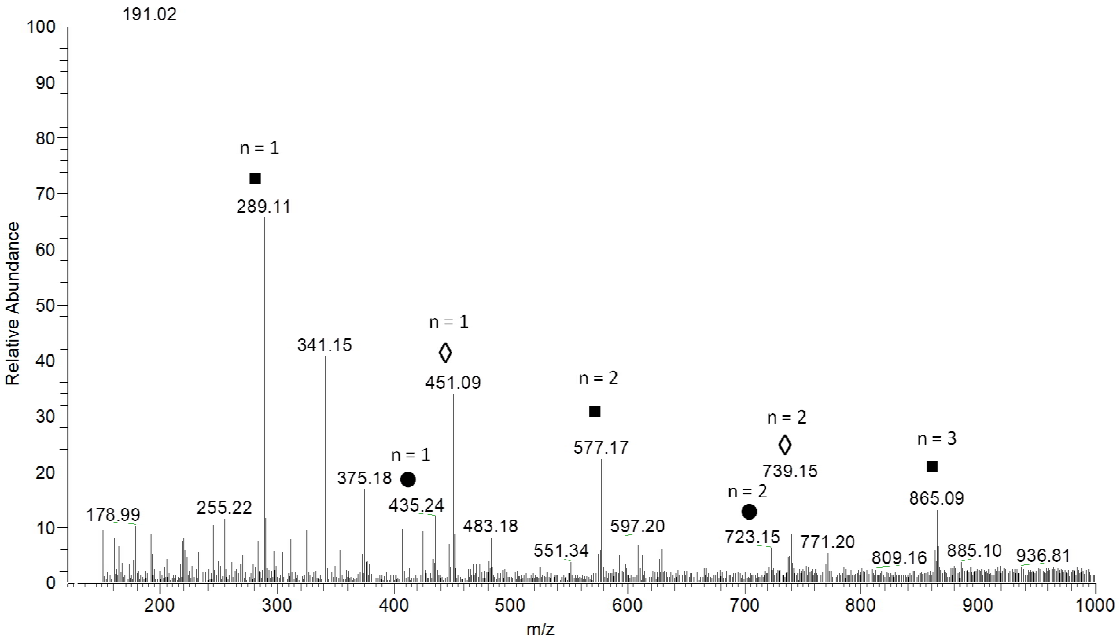

Figure 2. First-order mass spectrum of the AERM evaluated in negative mode ionization. n = number of catechins units; ▪ catechin derivatives; ● deoxyhex-catechin derivatives; ◊ hexose-catechin derivatives.

Table 1. *m/z* $[M–H]^-$ ion, MS^n fragments of the compounds obtained by FIA-ESI-IT-MS/MS of the AERM.

m/z [M-H]⁻	MS²	MS³	Proposed name
289	137 [M-152-H]⁻		catechin
435	283 [M-152-H]⁻	137 [M-152-146-H]⁻	catechin + deoxyhexose
451	299 [M-152-H]⁻	137 [M-152-162-H]⁻	catechin + hexose
515	353 [M-162-H]⁻	191 [M-162-162-H]⁻	dicaffeoyl quinic acid
577	451 [M-126-H]⁻		catechin dimer
	425 [M-152-H]⁻		
	289 [M-288-H]⁻		
609	463 [M-146-H]⁻		rutin
	301 [M-308-H]⁻		
723	571 [M-152-H]⁻	419 [M-152-H]⁻	catechin dimer + deoxyhexose
739	587 [M-152-H]⁻	569 [M-18-H]⁻	catechin dimer + hexose
		435 [M-152-H]⁻	
865	577 [M-288-H]⁻	451 [M-126-H]⁻	catechin trimer
		425 [M-152-H]⁻	
		289 [M-288-H]⁻	
1153	865 [M-288-H]⁻	847 [M-18-H]⁻	catechin tetramer
		739 [M-126-H]⁻	
		587 [M-278-H]⁻	
		577 [M-288-H]⁻	
		451 [M-414-H]⁻	

Preprints (www.preprints.org) | NOT PEER-REVIEWED | Posted: 9 April 2018 doi:10.20944/preprints201804.0100.v1

The MS^2 spectrum of the ion at *m/z* 577 (Figure 3A) showed major fragments at *m/z* 451, 425 and 289. The ion at *m/z* 451 arises from the loss of 126 mass units, corresponding to the HRF fragmentation. The ion of *m/z* 425 derived of the loss of 152 Da from the precursor ion of *m/z* 577, and it was proposed as arising from a RDA fragmentation. Whereas the fragment at *m/z* 289 $[M-288-H]^-$ was assigned to a QM fragmentation of the catechin dimer. These fragmentation patterns were previously described [24] and corroborate with the presence of PAs.

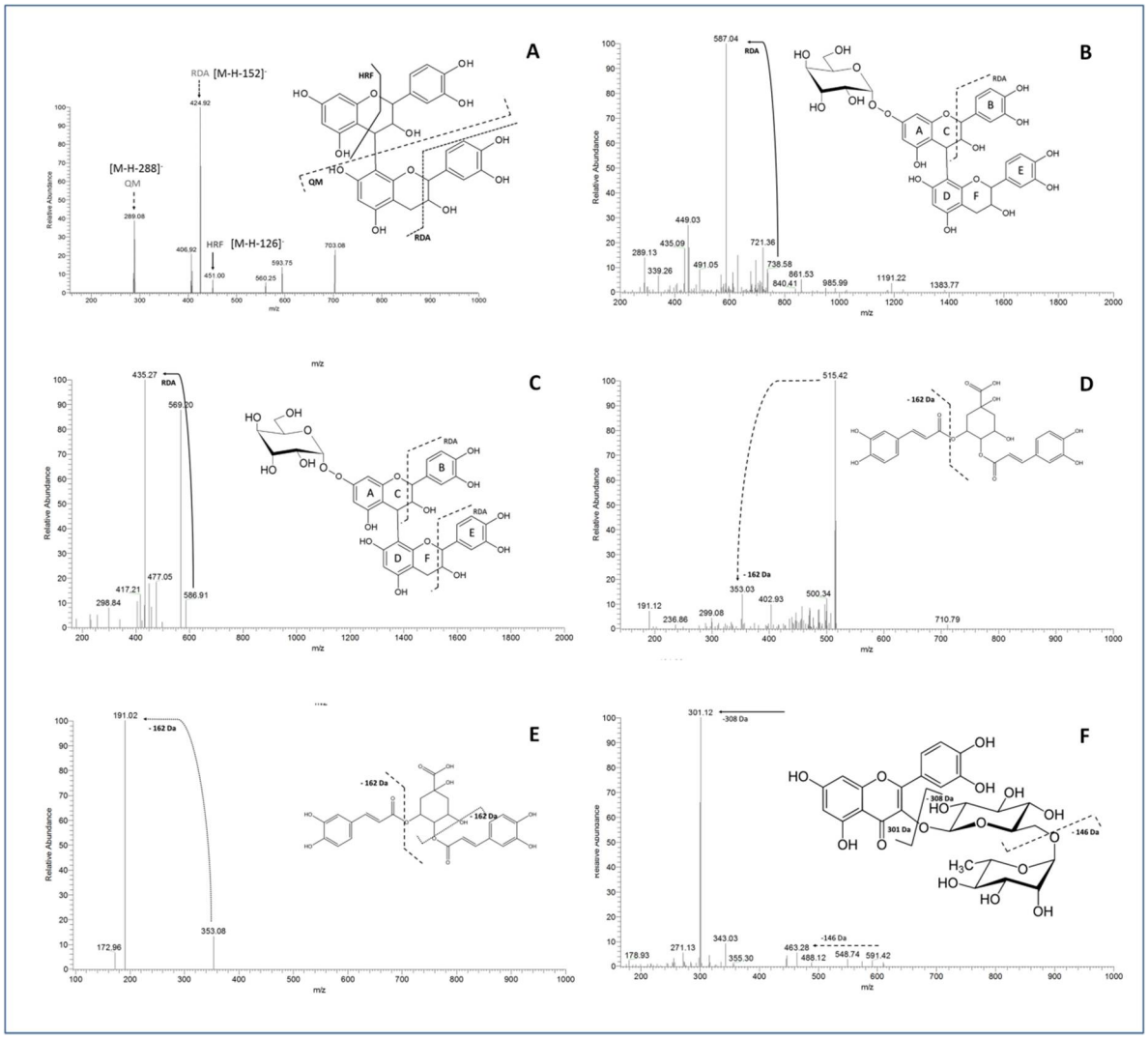

Figure 3. MS/MS spectra of the precursor ions representing the fragmentation pathways. (A) catechin dimer: *m/z* 577; (B-C) catechin dimer hexoside: *m/z* 739; (D-E) dicaffeoyl-quinic acids: *m/z* 353; (F) rutin: *m/z* 609

The series of PA containing hexose-catechins was also investigated using the same approach. The MS^2 spectrum of the ion of *m/z* 739 generated the product ion at *m/z* 587 $[M-152-H]^-$, due to a RDA fragmentation (Figure 3B), followed by another RDA $[M-152-152-H]^-$ fragmentation, generating the ion at *m/z* 435 (Figure 3C). This fragmentation pattern allowed us to presume the position of the sugar moiety either at ring A or D (Figure 3B-C). Similar fragmentation patterns occur with the third series of PA containing a deoxyhexose moiety (*m/z* 435 and *m/z* 723).

However, we observed that this type of fragmentation pattern does not occur with higher molecular weight molecules, such as catechin tetramers (*m/z* 1153). The MS^2 spectrum of the precursor ion at *m/z* 1153 generated the product ion at *m/z* 865 $[M-288-H]^-$, due to the QM fragmentation (Figure 4). The MS^3 spectrum of the precursor ion at *m/z* 1153 $[M-288-H]^-$ showed major product ions at *m/z* 847, *m/z* 739, *m/z* 587 and *m/z* 451 (Figure 4). The product ion at *m/z*

Preprints (www.preprints.org) | NOT PEER-REVIEWED | Posted: 9 April 2018 doi:10.20944/preprints201804.0100.v1

847 was derived from loss of water [M-18-H]$^-$. The product ion at *m/z* 739 was due to HRF [M-126-H]$^-$. HRF + RDA yielded the product ion at *m/z* 587 [M-278-H]$^-$; and the product ion at *m/z* 451 was generated from a QM + HRF fragmentation [M-414-H]$^-$. Figure 4 shows the fragmentation pathway proposed for the molecules of higher molecular weight, which have mixed fragmentations, not detected in smaller molecules.

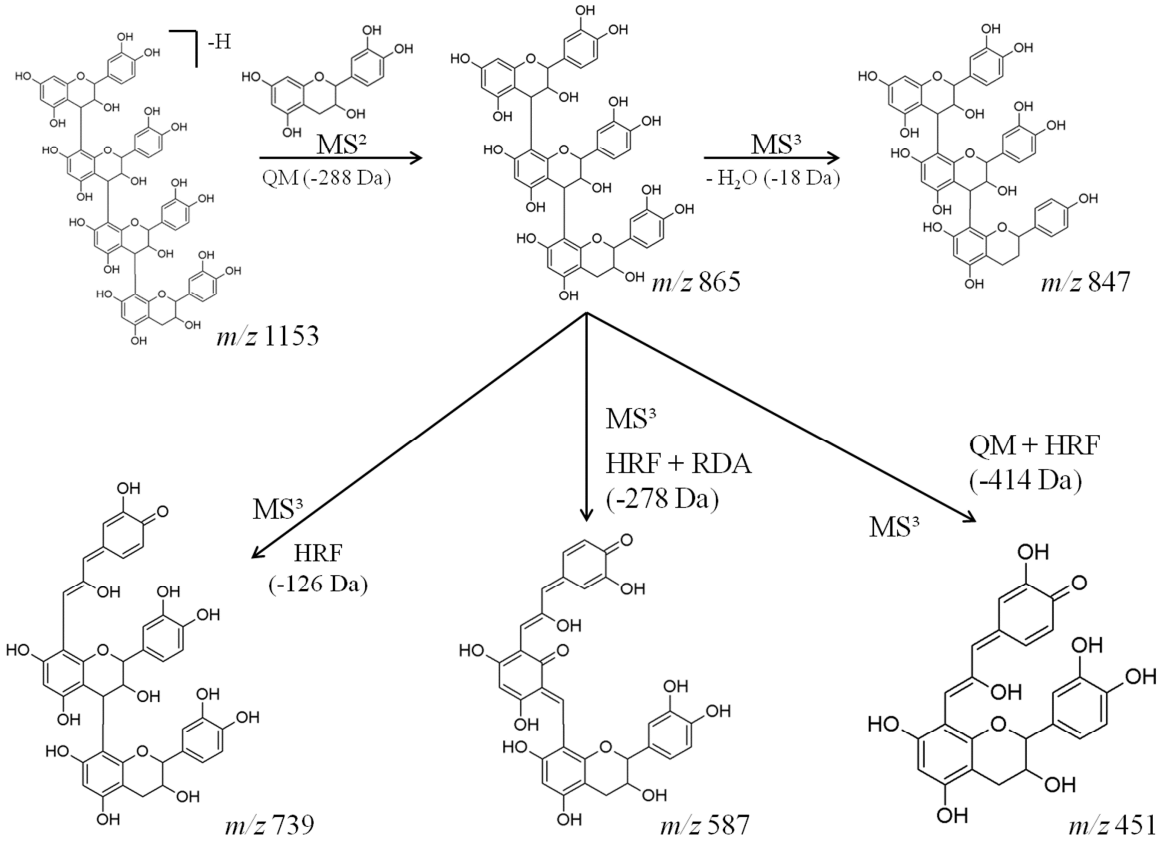

Figure 4. Fragmentation pathways of a possible tetramer proanthocyanidin found in AERM. The main fragmentation mechanisms involved are: HRF, RDA and QM.

Although the AERM is composed mostly of catechin derivatives, other substances were detected. Quinic acid derivatives (*m/z* 191) were detected in the negative mode. MS^2 fragmentation of the precursor ion at *m/z* 515 generated the product ion at *m/z* 353 [M-162-H]$^-$ (Figure 3D, Table 1). The MS^3 fragmentation of the precursor ion of *m/z* 515 produced the product ion of *m/z* 191 [M-162-162-H]$^-$ (Figure 3E, Table 1), characteristic of dicaffeoyl-quinic acids [25]. Probably, these substances are produced due to biotic and abiotic stress conditions in which the plant is submitted in the ecosystem [25]. In addition, this class of compounds has antioxidant, antiviral, anti-bactericidal, anti-inflammatory, cardiovascular risk reduction, diabetes type 2 and Alzheimer's disease beneficial role [26]. In our knowledge, this class of substances had not been reported in the literature for the genus *Rhizophora*.

Another substance detected by FIA-ESI-IT-MS/MS presented *m/z* 609. The MS^2 fragmentation of the precursor ion *m/z* 609 produced two major fragments. The ion at *m/z* 463 [M-146-H]$^-$ (Figure 3F) probably is due to the loss of a deoxyhexose moiety, whereas the ion at *m/z* 301 [M-308-H]$^-$ (Figure 3F) arises from the loss of a glycosidic hexose-deoxyhexose chain, which led us to propose the presence of rutin, a flavonoid commonly found in several plant families, which was already detected in the extracts of *R. mangle* [27].

2.2. *In vitro* activities of the AERM

The relatively stable organic radical ABTS$^{\bullet+}$ has been widely used for the determination of the radical scavenging of different plant extracts [28]. AERM showed intense antioxidant activity (608.8

 doi:10.20944/preprints201804.0100.v1

μmol Trolox/g). [19] reported powerful antioxidant activity of *R. mangle* and *R. mucronata* ethanolic extracts using the DPPH assay and attributed this effect to the large amount of condensed tannins present in the extract. Takara et al. (2008) [29] evaluated the antioxidant activity of the *R. stylosa* species and showed that the sugar moieties present in the condensed tannins further increase the efficiency of free radical sequestration, which might happens in the extract of the barks of *R. mangle*.

The digestion of food starch and triglycerides in gastrointestinal milieu is performed by amylases and lipases, respectively. Acarbose is widely recognized as a potent inhibitor of amylases and it delays the production of glucose helping to improve insulin resistance and glucose homeostasis in diabetic patients [30]. In the same line, Orlistat is a pancreatic lipase inhibitor currently approved as anti-obesity therapeutic by reducing the intestinal absorption of free fatty acids [31]. The presence of lipase and/or amylase inhibitors from plant origins has been demonstrated for different polyphenolic-rich plant species [32]. AERM demonstrate inhibitory lipase activity with IC50 = 803 μg/mL while Orlistat inhibit lipase with IC50=27.4 μg/mL in the same set of assays. Alpha-amylase assay also demonstrate an inhibitory activity of AERM with IC50=19.0 μg/mL, while acarbose inhibit amylase with IC50=5.2 μg/mL in the same set of assays. Tannins were pointed as potent inhibitors of the human salivary and porcine pancreatic α-amylases in previous studies [33,34], suggesting that PAs from AERM could be implicated in this potent inhibitory activity.

2.3 *In vivo* activities of the AERM

Mice fed during 8 weeks with high-fat diet becomes obese when compared with mice fed with standard diet, that can be observed by the increase in the final body weight and by the increase of the visceral and subcutaneous adipose tissue depots (Table 2). An increased of liver weight was also observed in the obese mice, suggesting the presence of hepatic alterations associated to obesity (Table 3). Four weeks treatment with AERM was not enough to statistically reduce the body weight gain and adiposity in HFD or control mice, but liver weight was significantly reduced in obese mice treated with *R. mangle* when compared to obese non-treated mice (Table 2).

Table 2. Body weight and body composition of control mice, control mice treated with AERM 5 mg.kg^{-1} (Control5) or 50 mg.kg^{-1} (Control50), obese mice (HFD) and obese mice treated with AERM 5 mg.kg^{-1} (HFD5) or 50 mg.kg^{-1} (HFD50).

parameters	Control	Control5	Control50	HFD	HFD5	HFD50
Body weight at 10th week (g)	42.2±1.4	41.7±1.2	43.0±1.8	55.0±1.2*	52.0±2.0	53.0±1.2
Final body weight (g)	44.7±1.8	45.2±1.6	43.5±1.3	61.2±2.4*	56.0±2.7	55.2±1.3
Δ Body weight (%)	5.8±1.2	8.2±1.5	1.6±2.5	9.8±2.6	6.2±2.7	4.2±2.2
Food intake (kcal/day)	14.3±1.1	13.3±0.4	12.0±0.4#	25.5±1.1	24.3±0.9	23.4±1.9
Epididimal fat (g)	1.8±0.3	1.5±0.2	1.5±0.1	2.7±0.1*	2.9±0.2	2.7±0.4
Epididimal fat (%)[a]	4.0±0.4	3.4±0.3	3.7±0.1	4.4±0.1	5.1±0.4	5.1±0.8
Subcutaneous fat (g)	0.7±0.1	0.5±0.1	0.6±0.1	1.3±0.1*	1.0±0.1	1.2±0.2
Subcutaneous fat (%)[a]	1.6±0.2	1.2±0.1	1.5±0.1	2.1±0.1*	1.8±0.3	2.2±0.2
Liver (g)	1.8±0.1	1.9±0.1	1.7±0.1	3.0±0.3*	2.1±0.1#	2.2±0.2#
Liver (%)[a]	4.2±0.2	4.2±0.1	4.0±0.1	4.9±0.3	3.7±0.3#	3.9±0.1#
Gastrocnemius muscle (g)	0.2±0.0	0.2±0.0	0.2±0.0	0.2±0.0	0.2±0.0	0.2±0.0
Gastrocnemius muscle (%)[a]	0.5±0.1	0.4±0.0	0.5±0.0	0.3±0.0	0.4±0.0	0.3±0.0

[a] % of body weight. * p<0.05 when compared with control group and # p<0.05 when compared with non-treated group. (n=5-6)

 doi:10.20944/preprints201804.0100.v1

Interestingly, glucose and insulin basal blood levels were also reduced in obese mice treated with AERM at higher dose employed (50 mg/kg), as well as, these mice were more tolerant to insulin, as we can observed by the kITT value (Table 3). Serum total and LDL-cholesterol were also reduced by AERM. Insulin resistance that results in hyperglycemia/hyperinsulinemia is routinely associated to obesity. Oral quercetin supplementation (30 mg/kg/day) was not effective for induce weight loss in HFD mice, but it was effective as an anti-diabetic biomolecule [35]. As demonstrated, oral ad libitum water administration with 0.5% of procyanidins from apple juice during 4 weeks to genetically obese mice results in maintenance of body weight and adiposity but also, improvements in insulin resistance via suppression of pro-inflammatory cytokines expression in liver [36].

Table 3. Serum parameters and kITT of control mice, control mice treated with AERM 5 $mg.kg^{-1}$ (Control5) or 50 $mg.kg^{-1}$ (Control50), obese mice (HFD) and obese mice treated with AERM 5 $mg.kg^{-1}$ (HFD5) or 50 $mg.kg^{-1}$ (HFD50).

	Control	Control5	Control50	HFD	HFD5	HFD50
Basal glucose (mg/dL)	166±5	150±4	152±5	226±11*	201±22	197±6#
Insulin (ng/mL)	106±13	112±14	207±16#	176±34*	161±17	127±9#
kITT	5.4±0.3	5.7±0.7	5.0±0.5	2.0±0.4*	2.6±0.8	3.2±0.3#
Total cholesterol (mg/dL)	174±2	164±2#	168±2	203±9*	184±7	180±4#
LDL-cholesterol (mg/dL)	100±7	98±6	102±6	144±10*	118±4#	106±9#
HDL-cholesterol (mg/dL)	57±4	54±3	52±1	52±2	50±1	54±2
Triglycerides (mg/dL)	187±22	193±32	201±24	99±7*	98±5	127±17

* $p<0.05$ when compared with control group and # $p<0.05$ when compared with non-treated group. (n=5)

The analysis of body composition, as cited above, revealed that obese mice treated with both AERM doses had liver weight reductions when compared with non-treated obese (Table 2). As we can observe, obese mice present steatosis after 14 weeks of high-fat diet, but in mice treated with AERM at dose of 50 mg/kg, hepatic steatosis area and triglycerides content is significantly reduced (Figure 5). However, in Swiss mice fed during 12 weeks with HFD no increased in hepatic pro-inflammatory cytokines gene expression (il-6, Tnf) were detected (Figure 6). In C57Bl6 strain, 12 weeks of HFD is not also able to induced inflammatory markers or JNK activation in liver. Hepatic inflammation was only observed when fructose or sucrose was added to HFD [37]. The hepatic triglycerides accumulation (steatosis) is the first step of NAFLD and could be due the increased free fatty acid (FFA) supply, decreased FFA oxidation, increased de novo lipogenesis and/or decreased very low-density lipoprotein (VLDL)-triglyceride secretion [38]. Liver uptake of FFA is facilitated by cell surface receptor as CD36/fatty acid translocase. The CD36 mRNA expression in hepatocytes is normally low, but an important increase is observed by a high-fat diet or by the activation of nuclear receptors including peroxisome proliferator-activated receptor (PPAR)-γ [39]. We can registered a modulatory effect of AERM in liver PPAR-γ mRNA expression associated to an important inhibition of CD36 mRNA expression (Figure 6A), suggesting that AERM induces the down regulation of CD36 mRNA via PPAR-gamma inhibition. Expression of *Srebf1* and *Pparα* that encode the sterol regulatory-binding protein-1c (SREBP-1c), a regulator of de novo lipogenesis, or PPAR-α, a regulator of FA oxidation was not altered in liver by AERM treatment. Herbal formulations as the aqueous extract of *Dolichos lablab*, the aqueous extracts of *Penthorum chinense*, ethanol extract of *Solidago virgaurea* or isolated flavonoid quercetin, for example, were also able to inhibits hepatic lipid accumulation trough the downregulation of mRNA expression of CD36 [40–43]. Several published data related that orlistat in a range of 10-100 mg/kg is able to reduce liver weight, hepatic triglycerides and serum triglycerides/cholesterol in mice fed with high-fat diet [44–46]. AERM demonstrated an *in vitro* anti-lipase activity less potent than orlistat, but an *in vitro* anti-amylase more potent than acarbose. *In vivo* orlistat administration requires doses not so inferior than used in

 doi:10.20944/preprints201804.0100.v1

our work for effective activity of AERM (50 mg/kg), as well as, acarbose *in vivo* is only effective at 40 mg/kg/day [47,48], suggesting that an anti-lipase and anti-amylase activity could be important in the lipid lowering, glucose homeostasis and hepatoprotective effects of AERM.

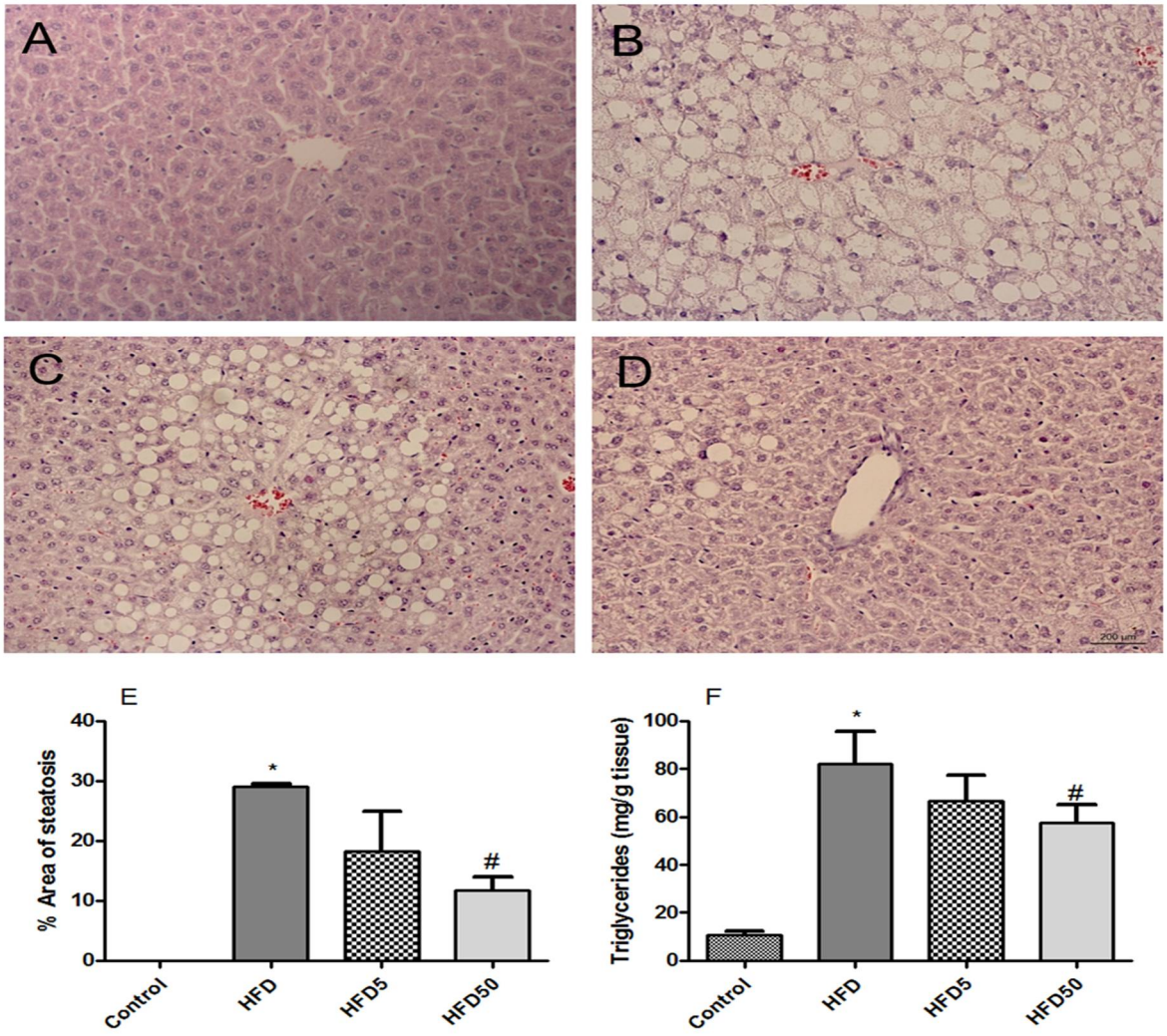

Figure 5. (A) Liver histology of control mice; (B) obese mice (HFD); (C) obese mice treated with AERM 5 mg.kg^{-1} (HFD 5); (D) obese mice treated with AERM 50 mg.kg^{-1} (HFD 50); (E) Steatosis measurement; (F) triglycerides content. Hematoxylin–eosin staining of 5.0 µm liver sections. Magnification: 200×. Steatosis measurement in 5 random power field of 5 mice per group. * $p < 0.01$ when compared with control group and # $p < 0.05$ when compared with HFD group (n=5).

Preprints (www.preprints.org) | NOT PEER-REVIEWED | Posted: 9 April 2018 doi:10.20944/preprints201804.0100.v1

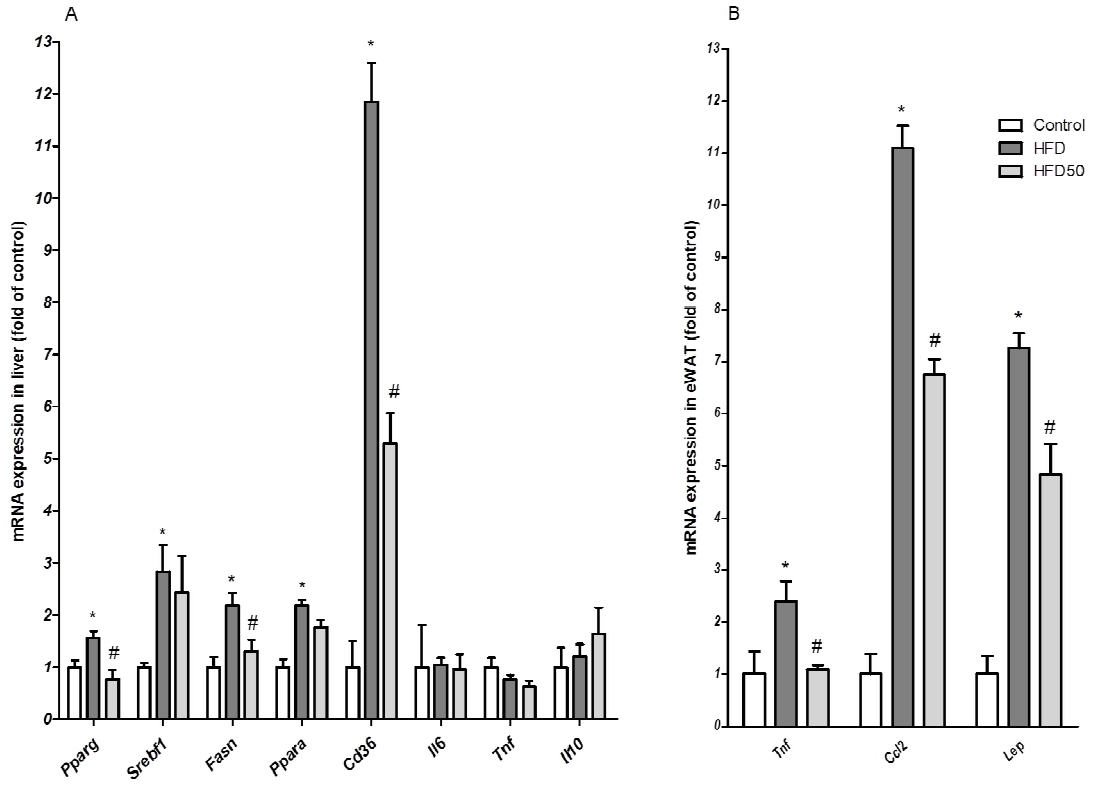

Figure 6. (A) mRNA expression in liver and (B) adipose tissue of control mice (Control), obese mice (HFD) and obese mice treated with AERM 50 mg.kg^{-1} (HFD50). * p<0.05 when compared with control group and # p<0.05 when compared with HFD group. (n=5)

Interestingly, mice treated with AERM did not present reduced adiposity but pro-inflammatory gene expression was reduced when compared with obese non-treated (Figure 6B), suggesting that AERM have anti-inflammatory activity mitigating obesity associated adipose tissue inflammation that could contribute to reverse the insulin resistance. Similar effect were previously described by dietary supplementation with procyanidins from grape-seed [49] and isolated catechins [50]. However, we search for antioxidant effects of AERM by measuring malondialdehyde (MDA) as index of lipid peroxidation [51] in liver and adipose tissue of mice and we was not able to confirm that antioxidant activity was maintained *in vivo* (data not shown).

The food ingestion was not different between obese groups. However, higher dose of AERM employed in our study was able to reduce the amount of food ingestion in the control group, as well as, the insulin basal level was elevated (Table 2). Insulin is able to signaling energy homeostasis to the central nervous system. Insulin and leptin levels are increased in individuals with obesity, but due the resistance to insulin present in these individuals, a dysregulation of satiety signaling occurs [52,53]. The AERM appetite suppression effect was only observed in lean mice, without insulin resistance, that central anorexigenic action of this protein is being performed correctly, but why AERM induces increases in insulin release should be further investigated. A tetrameric procyanidin from cacao, cinnamtannin A2, demonstrated an incretin activity, by increasing insulin release after oral administration to lean mice by mechanisms involving the increase plasma level of glucagon-like peptide (GLP)-1 [54].

 doi:10.20944/preprints201804.0100.v1

3. Materials and Methods

3.1 Sample taxon

The barks of *Rhizophora mangle* L. (Rhizophoraceae) were collected from the estuarine system of ecological station of Juréia-Itatins (Peruíbe, São Paulo - Brazil - 24º25'40''S – 47º05'20''W). The collected material had prior authorization from the Brazilian authorities (IBAMA/MMA: 52497-1). A voucher specimen (n° 11459) has been deposited at the Herbarium HUSC of the Santa Cecilia University (Santos, São Paulo - Brazil).

3.2 Chemical characterization

3.2.1 Preparation of plant extract: AERM

Fresh barks of *R. mangle* were washed, shade dried, powdered in a knife mill and sieved through a #60 mesh sieve. The powder (50 g) was extracted with 0.5 L of acetone (70% v/v) and macerated for seven days at room temperature (24°C), protected from light. The macerate was filtered through Whatman N°.1 filter paper and concentrated in a rotary flash evaporator at a temperature not exceeding 35°C. The extract (7 g, 14 %) was lyophilized and stored in amber bottles and allocated in a freezer (-40 °C). In order to minimize the interference of very high order polymeric compounds, a solid-phase extraction (SPE) was made. An aliquot (10 mg) of the extract was submitted to the SPE using RP18 cartridge, eluted with H_2O/MeOH 8:2 (v/v) (5 mL). The eluate was filtered through the nylon membrane (0.22 μm) and directly analyzed by HPLC-PDA and ESI-IT-MS/MS.

3.2.2 HPLC-PDA

The chemical composition of AERM was investigated by high performance liquid chromatography coupled to a Photodiode Array Detector (HPLC-PAD), using a Jasco (Tokyo, Japan) HPLC equipped with a PU-2089 quaternary solvent pump, a MD-2010 PAD and an AS-2055 autosampler. The analytical column maintained at room temperature (25 °C), was a Phenomenex Synergi Hydro RP18 (250 mm × 4.6 mm H × i.d.; 4 μm) with a Phenomenex security guard column (4.0 mm × 2.0 mm). Separation of phenolic acids, flavonoids, flavan-3-ols and PA was established using the mobile phase of water (eluent A) and acetonitrile (eluent B), solvent A containing 0.1% formic acid, with the following gradient program: 5–50% B (30 min), 30-85% B (30-35 min), isocratic 85% B (45 min), 85–100% B (45-70 min), return to 5% B (2 min), and the column was reequilibrated with the initial conditions for 18 min before the next injection. The flow rate was 1.0 mL.min^{-1}, and the total run time was 70 min. EZChrom Elite Data System software (Chromatec, Idstein, Germany) was used for detection operation and data processing. The identification of the compounds was performed by retention time comparison and UV spectral analyses.

3.2.3 FIA-ESI-IT-MS/MS

Flow injection analysis (FIA) was performed using a Thermo Fisher Scientific ion trap mass spectrometer (San Jose, CA, USA) equipped with an electrospray ionization source. The MS and MS/MS analysis in negative ion mode were selected after calibration infusing a standard solution of (+)-catechin (1 μg.mL^{-1} in methanol) at a flow rate of 5 μL·min^{-1} and working under the following conditions: capillary voltage −31 V, spray voltage 5 kV, tube lens offset 75 V, capillary temperature 300 °C, sheath gas (N_2) flow rate 8 (arbitrary units). Negative ion mass spectra were recorded in the range *m*/*z* 100–2000 Da. The first event was a full scan mass spectrum to acquire data on ions in the *m*/*z* range. The second scan event was an MS/MS experiment performed by using data-dependent scan that was carried out on deprotonated molecules from the compounds at collision energy of 25-30% and activation time of 30 ms. Data acquisition and processing were performed using the Xcalibur software.

 doi:10.20944/preprints201804.0100.v1

3.3 *In vitro* assays

3.3.1 Trolox Equivalent Antioxidant Capacity (TEAC) Assay

The 2,2'-azino-bis(3-ethylbenzothiazoline-6-sulphonic acid) (ABTS) and potassium persulfate were dissolved in distilled water to a final concentration of 7 mM and 2.45 mM respectively. These two solutions were mixed and the mixture allowed to stand in the dark at room temperature for 16 h before use in order to produce ABTS radical (ABTS•+). For the study of phenolic compounds the ABTS radical solution was diluted with distilled water to an absorbance of 1.00 at 734 nm. Phenols (final concentrations 0.0001-0.01 mg/ml) or Trolox standards (final concentration 0-20 mM) were added to diluted ABTS•+ solution and the absorbance reading was taken 6 min after mixing using the spectrophotometer. Results are presented as the ability of phenols to scavenge of free radical ABTS • + (Trolox equivalent antioxidant capacity).

3.3.2 Lipase activity assay

The lipase activity was determined by measuring the release of p-nitrophenol from p-nitrophenyl palmitate (4-NPP) by using a spectrophotometric method at 405 nm. Lipase (10 mg/ml) from porcine pancreas type II (Sigma) was dissolved in reaction buffer 50 mM Tris–HCl pH 8.0, and then centrifuged at 5,500 rpm for 5 min to remove the insoluble components. 4-NPP was dissolved in 1:9 v/v isopropanol:reaction buffer (50 mM Tris–HCl pH 8,0 containing 0.1 % arabic gum and 0.4 % de triton x-100). The final reaction mixture was 1:2:1 v/v of AERM:pancreatic lipase solution:4-NPP (10 mM) was added into the 96-well microplate well and incubated at 37 °C for 20 min to measure the amount of 4-nitrophenol released. Orlistat was used as a positive control. Each experiment was carried out in triplicate. The lipase inhibition was expressed as percentage and IC50 calculated by using GraphPad Prism Software.

3.3.3 Alpha-amylase activity assay

The α-amylase activity was quantified by the reduction of 3,5-dinitrosalicylic acid to 3-amino-5-nitrosalicylic acid. The α-amilase (10 mg/ml) from porcine pancreas type VI-B (Sigma) was dissolved in buffer Tris–HCl 50 mM pH 7.0 containing NaCl 38 mmol/L e CaCl2 0,1 mmol/L. The reaction was composed with 0.1 % potato starch (w/v) as substrate, incubated at 37 °C for 20 min with AERM and α-amilase solution. The reaction was interrupted with the addition of 3,5-dinitrosalicylic acid (DNS), heated at 100°C for 5 min, prior to quantification by spectrophotometry at 540 nm. The activity was calculated using a standard curve of glucose as a reference. Acarbose was used as positive control. This experiment was carried out in triplicate. The a-amylase inhibition was expressed as percentage and IC50 calculated by using GraphPad Prism Software.

3.4 Experimental model of diet-induced obesity

3.4.1 Animals

Six-week-old Swiss male mice, free of specific pathogens, were obtained from the Multidisciplinary Center for Biological Research (CEMIB; State University of Campinas, Campinas, SP, Brazil). Experiments were performed in accordance with the principles outlined by the National Council for the Control of Animal Experimentation (CONCEA, Brazil) and received approval from the Ethics Committee of São Francisco University, Bragança Paulista, SP, Brazil (Protocol 001.02.16). Animals were maintained on a 12:12 h artificial light–dark cycle with humidity and temperature controlled.

3.4.2Diet-induced obesity and *R. mangle* treatment

After random selection, mice were introduced to commercial chow (Control; 5% energy from fat) or high-fat diets (HFD; 60% energy from fat) as previously described [55]. Body weights were assessed weekly. After 8 weeks, the control and HFD animals were randomly divided in groups (n = 5 each). During the next four weeks, mice received orally by gavage 5 or 50 mg/kg/day of AERM dissolved in filtered tap water adjusted in a final volume of 4 mL/kg. The food intake was monitored

 doi:10.20944/preprints201804.0100.v1

by subtracting the amount of food consumed from the volume offered to the animals during the AERM treatment.

3.4.3 Blood glucose levels and insulin tolerance tests

In the last day of AERM treatment, mice were deprived of food for 6 h and a blood drop was collected from their tails. Glucose was measured using the glucometer (Accutrend Plus, Roche Diagnostics, Mannheim, Germany). The insulin tolerance test was performed and calculated as previously described [55]. Results were expressed as kITT.

3.4.4Necropsy and sample collection

Mice were fasted for 6 h and anesthetized by xylasine/ketamine overdose (0.1 mL/30 g body weight of 1:1 v/v of 2 % xylasine and 10% ketamine). Blood was collected by cardiac puncture. Adipose tissue depots (epididymis and subcutaneous), liver and gastrocnemius muscle were carefully dissected, weighted and expressed as a percentage of body weight (b.w.). Liver and visceral adipose samples were collected and stored at -80 °C for further analyses.

3.4.5 Hepatic analyses

Hydrated 5.0 μm sections of paraformaldehyde-fixed, paraffin embedded liver specimens were stained using the hematoxylin–eosin method to evaluate the presence of liver steatosis. Steatosis quantification was performed by counting steatosis (macrovesicular and microvesicular) against a grid of 144 points. For the total lipid extractions, liver samples were homogenized in NaCl 0.9 % and after a chloroform and methanol misture (2:1 v/v) was added [56]. The chloroform layer was collected, dried under N_2 and reconstituted in PBS buffer. Triglycerides and total cholesterol were measured using commercial kit (Laborlab, MG, Brazil).

3.4.6. Serum analyses

Serum triglycerides and total-, LDL- and HDL-cholesterol were measured using commercial kits (LaborLab, MG, Brazil). Insulin was quantified using Milliplex kit (Merck Millipore, USA).

3.4.7. Quantitative real-time polymerase chain reaction (qPCR)

The relative expression levels of different genes in the liver and adipose tissue samples were quantified by real-time polymerase chain reaction (PCR) as described previously [57]. All the data (analysed by ΔΔCt method) were normalized to control gene (18S) and represented as fold change with respect to Control group. Primers used were listed in Table 4.

Table 4. Primers used for real-time PCR.

Gene	Primer	Sequence (5′ → 3′)
Pparg	Sense	GATGGAAGACCACTCGCATT
	Antisense	AACCATTGGGTCAGCTCTTG
Ppara	Sense	AGAAGTTGCAGGAGGGGATT
	Antisense	TTGAAGCAGCTTYGGGAAGA
Srebf1	Sense	GTGAGCCTGACAAGCAATCA
	Antisense	GGTGCCTACAGAGCAAGAGG
Cd36	Sense	ATTCTCATGCCAGTCGGAGA

 doi:10.20944/preprints201804.0100.v1

	Antisense	TGGCTTTTGCACATCAAAGA
Tnf	Sense	TAGCCAGGAGGGAGAACAGA
	Antisense	TTTTCTGGAGGGAGATGTGG
Ccl2	Sense	CCCAATGAGTAGGCTGGAGA
	Antisense	TCTGGACCCATTCCTTCTTG
Lep	Sense	CTATGCCACCTTGGTCACCT
	Antisense	ACCAAACCAAGCATTTTTGC
Il10	Sense	ATCGATTTCTCCCCTGTGAA
	Antisense	TTCATGGCCTTGTAGACACCT
Il6	Sense	TCTCTGGGAAATCGTGGAA
	Antisense	TTCTGCAAGTGCATCATCG
Fasn	Sense	CACAGATGATGACAGGAGATGGA
	Antisense	TCGGAGTGAGGCTGGGTTGATA
18s	Sense	AAACGGCTACCACATCCAAG
	Antisense	CAATTACAGGGCCTCGAAAG

3.5 Statistical analyses

The results were expressed as the means ± standard errors of the mean (SEM). Statistically significant differences were determined using analysis of variance (ANOVA) followed by Dunnett's test for multiple comparisons using GraphPad Instat (GraphPad Software, Inc**.,** La Jolla, CA, USA). p values < 0.05 were considered to be significant.

4. Conclusions

In summary, the data obtained evidenced the presence of three series of PAs from 1 up to 4 catechin moieties and their glycosylated forms, besides phenolic acids and flavonoids, in the acetonic extract of the barks of *R. mangle*, which displayed antioxidant, anti-lipase and anti-amylase activity *in vitro*. In vivo, the barks extract of *R. mangle* displayed hepatoprotective and lipid lowering effects associated with reversion of insulin resistance and adipose tissue inflammation associated to obesity. Taken together, these results support the traditional knowledge about the use of *R. mangle* for the treatment of type 2 diabetes and reveal the potential of bark extract for the treatment of NAFLD and management of obesity associated alterations.

Acknowledgments: We thank the "Fundação de Amparo a Pesquisa do Estado de São Paulo- FAPESP" for fundings (2009/52237-9) and fellowships (2014/23113-0).

 doi:10.20944/preprints201804.0100.v1

Author Contributions: L.M.S.M, C.Q.R. A.G. and W.V: wote the manuscript, chemical characterization, *in vitro* and *in vivo* assays; C.R.P.C, P.S.S, C.C.R, N.S.L, D.K.T.M: wrote the manuscript and *in vivo* assays; D.C.M and V.V.R: wrote the manuscript and *in vitro assays*

Conflicts of Interest: "The authors declare no conflict of interest."

Abbreviations

ABTS	2,2'-azino-bis(3-ethylbenzothiazoline-6-sulphonic acid)
AERM	Acetonic extract of *Rhizophora mangle* barks
HPLC-PDA	High performance liquid chromatography coupled to photodiode array
HFD	High fat diet
HRF	Heterocyclic ring fission
FIA-ESI-IT-MS	Flow injection analysis electrospray-ion trap mass spectrometry
kiTT	Insulin tolerance test
m/z	mass/charge ratio
NAFLD	Non-alcoholic fatty liver disease
PAs	Proanthocyanidins
RDA	Retro Diels-Alder
QM	Quinone-methide

References

1. World Health Organization *Global report on diabetes*; World Health Organization, 2016; ISBN 92-4-156525-X.
2. ABESO *Mapa da obesidade*; Brazilian Association for obesity study; 2017.
3. Zhang, Y.; Feng, F.; Chen, T.; Li, Z.; Shen, Q. W. Antidiabetic and antihyperlipidemic activities of Forsythia suspensa (Thunb.) Vahl (fruit) in streptozotocin-induced diabetes mice. *Journal of ethnopharmacology* **2016**, *192*, 256–263.
4. Choudhury, H.; Pandey, M.; Hua, C. K.; Mun, C. S.; Jing, J. K.; Kong, L.; Ern, L. Y.; Ashraf, N. A.; Kit, S. W.; Yee, T. S. An update on natural compounds in the remedy of diabetes mellitus: A systematic review. *Journal of Traditional and Complementary Medicine* **2017**.
5. Zhang, L.; Mao, W.; Guo, X.; Wu, Y.; Li, C.; Lu, Z.; Su, G.; Li, X.; Liu, Z.; Guo, R. Ginkgo biloba extract for patients with early diabetic nephropathy: a systematic review. *Evidence-Based Complementary and Alternative Medicine* **2013**, *2013*.
6. Valdivia-Correa, B.; Gómez-Gutiérrez, C.; Uribe, M.; Méndez-Sánchez, N. Herbal medicine in Mexico: a cause of hepatotoxicity. A critical review. *International journal of molecular sciences* **2016**, *17*, 235.
7. Andrade-Cetto, A.; Heinrich, M. Mexican plants with hypoglycaemic effect used in the treatment of diabetes. *Journal of ethnopharmacology* **2005**, *99*, 325–348.
8. Alarcon-Aguilara, F.; Roman-Ramos, R.; Perez-Gutierrez, S.; Aguilar-Contreras, A.; Contreras-Weber, C.; Flores-Saenz, J. Study of the anti-hyperglycemic effect of plants used as antidiabetics. *Journal of ethnopharmacology* **1998**, *61*, 101–110.
9. Nebula, M.; Harisankar, H.; Chandramohanakumar, N. Metabolites and bioactivities of Rhizophoraceae mangroves. *Natural products and bioprospecting* **2013**, *3*, 207–232.
10. Azman, A.-S.; Othman, I.; S Velu, S.; Chan, K.-G.; Lee, L.-H. Mangrove rare actinobacteria: taxonomy, natural compound, and discovery of bioactivity. *Frontiers in microbiology* **2015**, *6*, 856.

11. de Faria, F. M.; Luiz-Ferreira, A.; Socca, E. A. R.; de Almeida, A. C. A.; Dunder, R. J.; Manzo, L. P.; da Silva, M. A.; Vilegas, W.; Rozza, A. L.; Pellizzon, C. H. Effects of Rhizophora mangle on experimental colitis induced by TNBS in rats. *Evidence-Based Complementary and Alternative Medicine* **2012**, *2012*.
12. Thring, T. S.; Hili, P.; Naughton, D. P. Antioxidant and potential anti-inflammatory activity of extracts and formulations of white tea, rose, and witch hazel on primary human dermal fibroblast cells. *Journal of Inflammation* **2011**, *8*, 27.
13. He, F.; Pan, Q.-H.; Shi, Y.; Duan, C.-Q. Biosynthesis and genetic regulation of proanthocyanidins in plants. *Molecules* **2008**, *13*, 2674–2703.
14. Jayarathne, S.; Koboziev, I.; Park, O.-H.; Oldewage-Theron, W.; Shen, C.-L.; Moustaid-Moussa, N. Anti-Inflammatory and Anti-Obesity Properties of Food Bioactive Components: Effects on Adipose Tissue. *Preventive nutrition and food science* **2017**, *22*, 251.
15. de-Faria, F. M.; Almeida, A. C. A.; Luiz-Ferreira, A.; Takayama, C.; Dunder, R. J.; da Silva, M. A.; Salvador, M. J.; Abdelnur, P. V.; Eberlin, M. N.; Vilegas, W. Antioxidant action of mangrove polyphenols against gastric damage induced by absolute ethanol and ischemia-reperfusion in the rat. *The Scientific World Journal* **2012**, *2012*.
16. Rohr, G. E.; Meier, B.; Sticher, O. Evaluation of different detection modes for the analysis of procyanidins in leaves and flowers ofCrataegus spp. Part I. Diode array and electrochemical detection. *Phytochemical Analysis* **2000**, *11*, 106–112.
17. Ravikumar, S.; Inbaneson, S. J.; Suganthi, P.; Venkatesan, M.; Ramu, A. Mangrove plants as a source of lead compounds for the development of new antiplasmodial drugs from South East coast of India. *Parasitology research* **2011**, *108*, 1405–1410.
18. Oo, C. W.; Pizzi, A.; Pasch, H.; Kassim, M. J. Study on the structure of mangrove polyflavonoid tannins with MALDI-TOF mass spectrometry. *Journal of Applied Polymer Science* **2008**, *109*, 963–967.
19. Zhang, L.-L.; Lin, Y.-M.; Zhou, H.-C.; Wei, S.-D.; Chen, J.-H. Condensed tannins from mangrove species Kandelia candel and Rhizophora mangle and their antioxidant activity. *Molecules* **2010**, *15*, 420–431.
20. Li, H.-J.; Deinzer, M. L. Tandem mass spectrometry for sequencing proanthocyanidins. *Analytical chemistry* **2007**, *79*, 1739–1748.
21. Fulcrand, H.; Mané, C.; Preys, S.; Mazerolles, G.; Bouchut, C.; Mazauric, J.-P.; Souquet, J.-M.; Meudec, E.; Li, Y.; Cole, R. B. Direct mass spectrometry approaches to characterize polyphenol composition of complex samples. *Phytochemistry* **2008**, *69*, 3131–3138.
22. Maldini, M.; Montoro, P.; Piacente, S.; Pizza, C. ESI-MS, ESI-MS/MS fingerprint and LC-ESI-MS analysis of proathocyanidins from Bursera simaruba Sarg bark. *Natural product communications* **2009**, *4*, 1671–1674.
23. Rodrigues, C. M.; Rinaldo, D.; dos Santos, L. C.; Montoro, P.; Piacente, S.; Pizza, C.; Hiruma-Lima, C. A.; Brito, A. R.; Vilegas, W. Metabolic fingerprinting using direct flow injection electrospray ionization tandem mass spectrometry for the characterization of proanthocyanidins from the barks of Hancornia speciosa. *Rapid Communications in Mass Spectrometry* **2007**, *21*, 1907–1914.
24. Tala, V. R. S.; Candida da Silva, V.; Rodrigues, C. M.; Nkengfack, A. E.; Campaner dos Santos, L.; Vilegas, W. Characterization of Proanthocyanidins from Parkia biglobosa (Jacq.) G.

Don.(Fabaceae) by Flow Injection Analysis—Electrospray Ionization Ion Trap Tandem Mass Spectrometry and Liquid Chromatography/Electrospray Ionization Mass Spectrometry. *Molecules* **2013**, *18*, 2803–2820.

25. Gouveia, S. C.; Castilho, P. C. Validation of a HPLC-DAD–ESI/MS n method for caffeoylquinic acids separation, quantification and identification in medicinal Helichrysum species from Macaronesia. *Food research international* **2012**, *45*, 362–368.
26. Farah, A.; Monteiro, M.; Donangelo, C. M.; Lafay, S. Chlorogenic acids from green coffee extract are highly bioavailable in humans. *The Journal of Nutrition* **2008**, *138*, 2309–2315.
27. Kandil, F.; Grace, M.; Seigler, D.; Cheeseman, J. Polyphenolics in Rhizophora mangle L. leaves and their changes during leaf development and senescence. *Trees* **2004**, *18*, 518–528.
28. Tirzitis, G.; Bartosz, G. Determination of antiradical and antioxidant activity: basic principles and new insights. *Acta Biochim Pol* **2010**, *57*, 139–42.
29. Takara, K.; Kuniyoshi, A.; Wada, K.; Kinjyo, K.; Iwasaki, H. Antioxidative flavan-3-ol glycosides from stems of Rhizophora stylosa. *Bioscience, biotechnology, and biochemistry* **2008**, *72*, 2191–2194.
30. Kim, M.-J.; Lee, S.-B.; Lee, H.-S.; Lee, S.-Y.; Baek, J.-S.; Kim, D.; Moon, T.-W.; Robyt, J. F.; Park, K.-H. Comparative study of the inhibition of α-glucosidase, α-amylase, and cyclomaltodextrin glucanosyltransferase by acarbose, isoacarbose, and acarviosine–glucose. *Archives of biochemistry and biophysics* **1999**, *371*, 277–283.
31. Tiss, A.; Ransac, S.; Lengsfeld, H.; Hadvàry, P.; Cagna, A.; Verger, R. Surface behaviour of bile salts and tetrahydrolipstatin at air/water and oil/water interfaces. *Chemistry and physics of lipids* **2001**, *111*, 73–85.
32. Martinez-Gonzalez, A. I.; Díaz-Sánchez, Á. G.; Rosa, L. A.; Vargas-Requena, C. L.; Bustos-Jaimes, I. Polyphenolic compounds and digestive enzymes: in vitro non-covalent interactions. *Molecules* **2017**, *22*, 669.
33. Kato, C. G.; Gonçalves, G. de A.; Peralta, R. A.; Seixas, F. A. V.; de Sá-Nakanishi, A. B.; Bracht, L.; Comar, J. F.; Bracht, A.; Peralta, R. M. Inhibition of α-amylases by condensed and hydrolysable tannins: focus on kinetics and hypoglycemic actions. *Enzyme research* **2017**, *2017*.
34. Kato, E.; Kushibiki, N.; Inagaki, Y.; Kurokawa, M.; Kawabata, J. Astilbe thunbergii reduces postprandial hyperglycemia in a type 2 diabetes rat model via pancreatic alpha-amylase inhibition by highly condensed procyanidins. *Bioscience, biotechnology, and biochemistry* **2017**, *81*, 1699–1705.
35. Arias, N.; Macarulla, M.; Aguirre, L.; Martinez-Castano, M.; Portillo, M. Quercetin can reduce insulin resistance without decreasing adipose tissue and skeletal muscle fat accumulation. *Genes & nutrition* **2014**, *9*, 361.
36. Ogura, K.; Ogura, M.; Shoji, T.; Sato, Y.; Tahara, Y.; Yamano, G.; Sato, H.; Sugizaki, K.; Fujita, N.; Tatsuoka, H. Oral Administration of Apple Procyanidins Ameliorates Insulin Resistance via Suppression of Pro-Inflammatory Cytokine Expression in Liver of Diabetic ob/ob Mice. *Journal of agricultural and food chemistry* **2016**, *64*, 8857–8865.
37. Luo, Y.; Burrington, C. M.; Graff, E. C.; Zhang, J.; Judd, R. L.; Suksaranjit, P.; Kaewpoowat, Q.; Davenport, S. K.; O'Neill, A. M.; Greene, M. W. Metabolic phenotype and adipose and liver features in a high-fat Western diet-induced mouse model of obesity-linked NAFLD. *American Journal of Physiology-Endocrinology and Metabolism* **2015**, *310*, E418–E439.

38. Tilg, H.; Moschen, A. R. Insulin resistance, inflammation, and non-alcoholic fatty liver disease. *Trends in Endocrinology & Metabolism* **2008**, *19*, 371–379.
39. Koonen, D. P.; Jacobs, R. L.; Febbraio, M.; Young, M. E.; Soltys, C.-L. M.; Ong, H.; Vance, D. E.; Dyck, J. R. Increased hepatic CD36 expression contributes to dyslipidemia associated with diet-induced obesity. *Diabetes* **2007**, *56*, 2863–2871.
40. Cao, Y.-W.; Jiang, Y.; Zhang, D.-Y.; Zhang, X.-J.; Hu, Y.-J.; Li, P.; Su, H.; Wan, J.-B. The hepatoprotective effect of aqueous extracts of Penthorum chinense Pursh against acute alcohol-induced liver injury is associated with ameliorating hepatic steatosis and reducing oxidative stress. *Food & function* **2015**, *6*, 1510–1517.
41. Im, A.-R.; Kim, Y. H.; Lee, H. W.; Song, K. H. Water extract of Dolichos lablab attenuates hepatic lipid accumulation in a cellular nonalcoholic fatty liver disease model. *Journal of medicinal food* **2016**, *19*, 495–503.
42. Pisonero-Vaquero, S.; Martínez-Ferreras, Á.; García-Mediavilla, M. V.; Martínez-Flórez, S.; Fernández, A.; Benet, M.; Olcoz, J. L.; Jover, R.; González-Gallego, J.; Sánchez-Campos, S. Quercetin ameliorates dysregulation of lipid metabolism genes via the PI3K/AKT pathway in a diet-induced mouse model of nonalcoholic fatty liver disease. *Molecular nutrition & food research* **2015**, *59*, 879–893.
43. Wang, Z.; Kim, J. H.; Jang, Y. S.; Kim, C. H.; Lee, J.-Y.; Lim, S. S. Anti-obesity effect of Solidago virgaurea var. g igantea extract through regulation of adipogenesis and lipogenesis pathways in high-fat diet-induced obese mice (C57BL/6N). *Food & nutrition research* **2017**, *61*, 1273479.
44. Jeong, E. J.; Jegal, J.; Ahn, J.; Kim, J.; Yang, M. H. Anti-obesity effect of Dioscorea oppositifolia extract in high-fat diet-induced obese mice and its chemical characterization. *Biological and Pharmaceutical Bulletin* **2016**, *39*, 409–414.
45. Ji, W.; Zhao, M.; Wang, M.; Yan, W.; Liu, Y.; Ren, S.; Lu, J.; Wang, B.; Chen, L. Effects of canagliflozin on weight loss in high-fat diet-induced obese mice. *PloS one* **2017**, *12*, e0179960.
46. Wu, T.; Yu, Z.; Tang, Q.; Song, H.; Gao, Z.; Chen, W.; Zheng, X. Honeysuckle anthocyanin supplementation prevents diet-induced obesity in C57BL/6 mice. *Food & function* **2013**, *4*, 1654–1661.
47. Lee, A.-Y.; Kang, M.-J.; Choe, E.; Kim, J.-I. Hypoglycemic and antioxidant effects of Daraesoon (Actinidia arguta shoot) in animal models of diabetes mellitus. *Nutrition research and practice* **2015**, *9*, 262–267.
48. Shen, K.-P.; Su, C.-H.; Lu, T.-M.; Lai, M.-N.; Ng, L.-T. Effects of Grifola frondosa non-polar bioactive components on high-fat diet fed and streptozotocin-induced hyperglycemic mice. *Pharmaceutical biology* **2015**, *53*, 705–709.
49. Terra, X.; Pallarés, V.; Ardèvol, A.; Bladé, C.; Fernández-Larrea, J.; Pujadas, G.; Salvadó, J.; Arola, L.; Blay, M. Modulatory effect of grape-seed procyanidins on local and systemic inflammation in diet-induced obesity rats. *The Journal of nutritional biochemistry* **2011**, *22*, 380–387.
50. Vazquez Prieto, M. A.; Bettaieb, A.; Rodriguez Lanzi, C.; Soto, V. C.; Perdicaro, D. J.; Galmarini, C. R.; Haj, F. G.; Miatello, R. M.; Oteiza, P. I. Catechin and quercetin attenuate adipose inflammation in fructose-fed rats and 3T3-L1 adipocytes. *Molecular nutrition & food research* **2015**, *59*, 622–633.

610 51. Draper, H.; Hadley, M. Malondialdehyde determination as index of lipid peroxidation.
611 Methods Ezymol. 1990; 86: 421-431.
612 52. Hamed, E. A.; Zakary, M. M.; Ahmed, N. S.; Gamal, R. M. Circulating leptin and insulin in
613 obese patients with and without type 2 diabetes mellitus: relation to ghrelin and oxidative
614 stress. *Diabetes research and clinical practice* **2011**, *94*, 434–441.
615 53. Karczewska-Kupczewska, M.; Strączkowski, M.; Adamska, A.; Nikołajuk, A.; Otziomek, E.;
616 Górska, M.; Kowalska, I. Increased suppression of serum ghrelin concentration by
617 hyperinsulinemia in women with anorexia nervosa. *European journal of endocrinology* **2010**, *162*,
618 235–239.
619 54. Yamashita, Y.; Okabe, M.; Natsume, M.; Ashida, H. Cinnamtannin A2, a tetrameric
620 procyanidin, increases GLP-1 and insulin secretion in mice. *Bioscience, biotechnology, and*
621 *biochemistry* **2013**, *77*, 888–891.
622 55. DeOliveira, C. C.; Acedo, S. C.; Gotardo, É. M. F.; de Oliveira Carvalho, P.; Rocha, T.;
623 Pedrazzoli, J.; Gambero, A. Effects of methotrexate on inflammatory alterations induced by
624 obesity: an in vivo and in vitro study. *Molecular and cellular endocrinology* **2012**, *361*, 92–98.
625 56. Folch, J.; Lees, M.; Sloane-Stanley, G. A simple method for the isolation and purification of
626 total lipids from animal tissues. *J biol Chem* **1957**, *226*, 497–509.
627 57. Z Nakamitsu, P.; M Compri, C.; de Fraia Pinto, L.; MF Gotardo, E.; C de Oliveira, C.; L Ribeiro,
628 M.; Pedrazzoli, J.; Gambero, A. Thalidomide controls adipose tissue inflammation associated
629 with high-fat diet-induced obesity in mice. *Endocrine, Metabolic & Immune Disorders-Drug*
630 *Targets (Formerly Current Drug Targets-Immune, Endocrine & Metabolic Disorders)* **2015**, *15*,
631 151–158.

632

633